Electronic Supplementary Information (ESI)

Collaborative Enhancement from Pb^{2+} and F^- in $Pb_2(NO_3)_2(H_2O)F_2$ Generates the Largest Second Harmonic Generation Effect Among Nitrates

Guang Peng,[ac] Yi Yang,[bc] Yu-Huan Tang,[ac] Min Luo,[a] Tao Yan,[a] Yuqiao Zhou,[ac] Chensheng Lin,[a] Zheshuai Lin,[b] and Ning Ye*[a]

[a] Key Laboratory of Optoelectronic Materials Chemistry and Physics, Fujian Institute of Research on the Structure of Matter, Chinese Academy of Sciences, Fuzhou, Fujian 350002, P. R. China.

[b] Beijing Center for Crystal R&D, Key Lab of Functional Crystals and Laser Technology of Chinese Academy of Sciences, Technical Institute of Physics and Chemistry, Chinese Academy of Sciences, Beijing 100190, P. R. China

[c] University of the Chinese Academy of Sciences, Beijing 100049, P. R. China

E-mail: nye@fjirsm.ac.cn

Table of Contents

Section S1 Materials and Methods

Reagents

BeO (99.5%) was purchased from Shanghai Chemical Dispensing Factory. Both $Pb(NO_3)_2$ (AR, 99.0%) and PbF_2 (AR, 99.0%) were purchased from Sinopharm. Nitric acid solution (AR, 65.0~68.0%) was purchased from Xilong Scientific Co., Ltd. All of the reagents were used as received without further treatment.

Synthesis

Crystal $Pb_2(NO_3)_2(H_2O)F_2$ was grown by the hydrothermal method. The mixture of BeO (0.25g, 0.01mol), $Pb(NO_3)_2$ (1.655g, 0.005mol), PbF_2 (1.84g, 0.0075mol), concentrated nitric acid solution (0.9 mL, 65.0~68.0%) and deionized water (10 mL) was sealed in an autoclave equipped with a Teflon liner (23mL) and heated at 220 ^oC for 5 days, and then slowly cooled to 25 ^oC at a rate of 5 $^oCh^{-1}$. The product was washed with ethanol and then dried in the air. Colorless and transparent flaky crystals of $Pb_2(NO_3)_2(H_2O)F_2$ were obtained in a yield of about 71% according to Pb.

Single-Crystal Structure Determination

Single crystal X-ray diffraction data for $Pb_2(NO_3)_2(H_2O)F_2$ was collected at room temperature on a Rigaku Mercury CCD diffractometer which was equipped with graphite-monochromatic Mo Kα radiation (λ = 0.71073 Å). A transparent flaky crystal was glued on the top of a glass fiber with epoxy for structure determination. The hemisphere of data was corrected using a narrow-frame method with ω-scan mode. By using the CrystalClear program, the data was integrated, and the intensities of which were corrected for Lorentz polarization, air absorption, and absorption attributable to the variation in the path length through the detector faceplate. Absorption corrections were also applied which were based on the Multiscan technique. The crystal structure of $Pb_2(NO_3)_2(H_2O)F_2$ was determined by the direct methods and refined by full-matrix least-squares fitting on F^2 using SHELX-97.[1] All non-hydrogen atoms were refined with anisotropic displacement parameters. The structure was verified using the ADDSYM algorithm from the program PLATON,[2] and no higher symmetries were found. Relevant crystallographic data and details of the experimental conditions for $Pb_2(NO_3)_2(H_2O)F_2$ are summarized in Table S1. Atomic coordinates and equivalent isotropic displacement parameters, selected bond lengths and angles and anisotropic displacement parameters for $Pb_2(NO_3)_2(H_2O)F_2$ are listed seriatim in Tables S2-S4.

Powder X-ray diffraction

X-ray diffraction pattern of polycrystalline powder was obtained on a Miniflex-600 powder X-ray diffractometer by using Cu Kα radiation (λ = 1.54059 Å) at room temperature in the angular range of 2θ=10−80° with a scan step width of 0.02° and a fixed time of 0.2 s.

Energy-dispersive X-ray Spectroscopy Analysis

Microprobe elemental analyses were performed on a field emission scanning electron microscope (FESEM, SU-8010) equipped with an energy dispersive X-ray spectroscope (EDS). A $Pb_2(NO_3)_2(H_2O)F_2$ crystal washed by alcohol has been collected and then mounted on a aluminum sample stage by use carbon conductive tape. Several regions on this crystal were tested with a focused beam of 20 kV accelerating voltage and 12μA emission current.

Thermal analysis

The thermogravimetric (TG) and differential thermal analysis (DTA) were conducted on a Netzsch STA449F3 simultaneous analyzer. Reference (Al_2O_3) and crystal samples (5−10 mg) were enclosed in Al_2O_3 crucibles and

heated from 30 to 900 °C at a rate of 10 °Cmin^{-1} under constant flow of nitrogen gas.

Infrared spectroscopy

The infrared spectrum was recorded on a Bruker VERTEX 70 Fourier transform infrared spectrometer in the range from 400 to 4000 cm^{-1}. The sample was mixed thoroughly with dried KBr in a mass ration of 1:100.

Diffuse reflectance and transmittance spectroscopy

The diffuse reflectance spectrum of the powder sample of $Pb_2(NO_3)_2(H_2O)F_2$ was measured at room temperature in the range of 190−2500 nm with $BaSO_4$ as the standard of 100 % reflectance. The UV-Visible transmittance spectrum was measured from 200 to 500 nm using an unpolished $Pb_2(NO_3)_2(H_2O)F_2$ crystal wafer. All the data were collected on a PerkinElmer Lamda-950 ultraviolet/visible/near-infrared spectrophotometer.

Second-harmonic generation

Polycrystalline second-harmonic generation (SHG) signals were measured by Kurtz-Perry method.[3] Since SHG efficiency has significant correlation with the particle size of crystal, the sample was ground and sieved into the following particle size ranges: 25-45, 45-62, 62-75, 75-109, 109-150, and 150-212 μm. Then the samples of different particle sizes were pressed between two rounded 1 mm thick sheet glasses with a 2 mm thick rubber ring interlayer containing an 8 mm diameter hole in the middle, which were tightly sheathed in an aluminous round box with an 8 mm diameter hole in the middle. Relevant comparisons had been made with the well-known SHG material KDP by grinding and sieving into the same particle size ranges. The measurements were performed on a 1064 nm Q-switched Nd:YAG laser under the same voltage. A cutoff filter was used to limit background flash-lamp light on the sample, and an interference filter (530 ± 10 nm) was used to select the second harmonic for detection with a photomultiplier tube attached to a RIGOL DS1052E 50 MHz oscilloscope. The ratio of the second-harmonic intensity outputs was calculated. No index-matching fluid was used in any of the experiments.

Computational methods

The calculations of band structure and density of states (DOS) were performed by CASTEP,[4] a plane-wave pseudopotential total energy package based on density functional theory (DFT).[5] The experimental crystal structure was used with the positions of the hydrogen atoms were generated geometrically. The functional developed by Perdew-Burke-Emzerhoff (PBE) functional within the generalized gradient approximation (GGA)[6] form was adopted to describe the exchange-correlation energy. It is well known that the energy band gaps calculated by standard DFT method are usually smaller than the measured values owing to the discontinuity of exchange-correlation energy. Thus, the PBE0[7] exchange-correlation functional has also been used for a better estimation of the energy band gap. The optimized norm-conserving pseudopotentials[8] in the Kleinman-Bylander[9] form for all the elements were used to model the effective interaction between atom cores and valence electrons. Pb $5d^{10}6s^26p^2$, N $2s^22p^3$, O $2s^22p^4$, F $2s^22p^5$ and H $1s^1$ electrons were treated as valence electrons, allowing the adoption of a relatively small basis set without compromising the computational accuracy. The high kinetic energy cutoff 900 eV and dense 5×2×5 Monkhorst-Pack[10] k-point meshes in the Brillouin zones were chosen. Because of the commonly underestimate of band gap by DFT, a scissor operator[11] (1.57 eV) was adopted to shift all the conduction bands to match the calculated band gaps with the measured values. Based on the scissor-corrected electron band structure, the imaginary part of the dielectric function was calculated according to the electron transition from the valence band (VB) to conduction band (CB). Consequently, the real part of the dielectric function is obtained by the Kramers-Kronig[12] transform and the refractive index is determined. The SHG coefficients d_{ij} were obtained by the formula developed by Lin's group[13].

Calculation of bond valence

The bond valence sums based on the theoretical hydrogenated crystal structure of $Pb_2(NO_3)_2(H_2O)F_2$ have been calculated using the formula

$$V_i = \sum_j S_{ij} = \sum_j \exp\{(r_0 - r_{ij}) / B\}$$

where S_{ij} is the bond valence associated with bond length r_{ij}. Parameters r_0 and B (usually 0.37) are empirically determined parameters.[14] The calculated bond valences for Pb, N, O and F atoms are summarized in Table S5.

Calculation of structural criterion (*C*)

The contribution of anionic groups $[NO_3]^-$ to the whole SHG coefficient can be calculated by calculating the structural criterion (*C*) based on the anionic group theory.[15] The macroscopic second-order susceptibility $\chi^{(2)}$ could be expressed by equation (1),

$$\chi_{ijk}^{(2)} = \frac{F}{V} \sum_P \sum_{i'j'k'} \alpha_{ii'} \alpha_{jj'} \alpha_{kk'} \beta_{i'j'k'}^{(2)}(P) \qquad P = [NO_3] \qquad (1)$$

where *F* is the correction factor of the localized field; *V* is the volume of the unit cell; $\alpha_{ii'}$, $\alpha_{jj'}$ and $\alpha_{kk'}$ are the direction cosines between the macroscopic coordinates of the crystal and the microscopic coordinates of $[NO_3]^-$ groups, and $\beta_{i'j'k'}^{(2)}(P)$ is the microscopic second-order susceptibility tensor of an individual group. Owing to the fact that $[NO_3]^-$ is a planar group in point group D_{3h}, there are only two nonvanishing second-order susceptibilities $\beta_{111}^{(2)} = \beta_{222}^{(2)}$ in the Kleinman approximation. Because the geometrical factor, g, can be derived from equation (2), equation (1) may be simplified according to the deduction process shown in ref. [16]:

$$\chi_{ijk}^{(2)} = \frac{F}{V} \cdot g_{ijk} \cdot \beta_{111}^{(2)}([NO_3]) \qquad (2)$$

In the case of unspontaneous polarization, the structural criterion *C* is defined as:

$$C = \frac{g}{n} \qquad (3)$$

where *n* is the number of $[NO_3]^-$ groups in a unit cell. Thus, the $\chi_{ijk}^{(2)}$ is proportional to the monocelled number density of the $[NO_3]^-$ groups (*n/V*) and the structural criterion (*C*).

Table S1. Crystal data and structural refinement for $Pb_2(NO_3)_2(H_2O)F_2$

formula	$Pb_2(NO_3)_2(H_2O)F_2$
formula mass (amu)	594.40
temp (K)	173(2)
λ(Å)	0.71073
crystal system	orthorhombic
space group	Amm2
a (Å)	5.1684(12)
b(Å)	15.051(3)
c (Å)	4.9061(12)
α (deg)	90
β (deg)	90
γ (deg)	90
V (Å^3)	381.64(15)
Z	2
ρ(calcd) (g/cm^3)	5.155
μ (mm^{-1})	44.109
F(000)	504
θ (deg)	2.71-27.42
index range	-6 ≤ h ≤ 6 -19 ≤ k≤ 19 -6 ≤ l ≤ 6
Reflections collected / unique	1455 / 504
Rint	0.0611
Completeness to θ = 27.42° (%)	99.6
GOF on F^2	0.986
R_1/wR_2 $[F_o^2 > 2\sigma(F_o^2)]$[a]	0.0335/0.0651
R_1/wR_2 (all data)	0.0361/0.0662
absolute structure parameter	0.00

[a] $R_1(F) = \sum||F_o| - |F_c||/\sum|F_o|$, $wR_2(F_o^2) = [\sum w(F_o^2 - F_c^2)^2/\sum w(F_o^2)^2]^{1/2}$.

Table S2. Atomic coordinates (×10^4) and equivalent isotropic displacement parameters (Å^2×10^3) for $Pb_2(NO_3)_2(H_2O)F_2$.

Atom	x	y	z	U(eq)
Pb(1)	0	3790(1)	14985(4)	22(1)
O(1)	-2881(18)	3126(7)	19900(60)	41(3)
O(2)	-5000	3827(9)	16710(30)	25(3)
O(3)	0	5000	17820(30)	20(5)
N(1)	-5000	3377(12)	18880(30)	23(4)
F(1)	2540(20)	5000	12680(20)	29(3)

U(eq) is defined as one third of the trace of the orthogonalized U_{ij} tensor.

Table S3. Selected bond lengths (Å) and angles (degrees) for $Pb_2(NO_3)_2(H_2O)F_2$

Pb(1)-O(3)	2.290(10)	O(1)-N(1)	1.263(13)
Pb(1)-F(1)	2.512(8)	O(2)-N(1)	1.26(2)
Pb(1)-F(1)#1	2.512(8)	O(2)-Pb(1)#3	2.720(4)
Pb(1)-O(2)#2	2.720(5)	O(3)-Pb(1)#1	2.290(10)
Pb(1)-O(2)	2.720(5)	N(1)-O(1)#4	1.263(13)
Pb(1)-Pb(1)#1	3.6416(13)	F(1)-Pb(1)#1	2.512(8)
O(3)-Pb(1)-F(1)	72.3(3)	F(1)#1-Pb(1)-Pb(1)#1	43.55(19)
O(3)-Pb(1)-F(1)#1	72.3(3)	O(2)#2-Pb(1)-Pb(1)#1	88.8(3)
F(1)-Pb(1)-F(1)#1	62.9(5)	O(2)-Pb(1)-Pb(1)#1	88.8(3)
O(3)-Pb(1)-O(2)#2	78.2(3)	N(1)-O(2)-Pb(1)#3	104.6(3)
F(1)-Pb(1)-O(2)#2	68.3(4)	N(1)-O(2)-Pb(1)	104.6(3)
F(1)#1-Pb(1)-O(2)#2	128.4(4)	Pb(1)#3-O(2)-Pb(1)	143.6(6)
O(3)-Pb(1)-O(2)	78.2(3)	Pb(1)-O(3)-Pb(1)#1	105.3(7)
F(1)-Pb(1)-O(2)	128.4(4)	O(2)-N(1)-O(1)#4	119.8(12)
F(1)#1-Pb(1)-O(2)	68.3(4)	O(2)-N(1)-O(1)	119.8(12)
O(2)#2-Pb(1)-O(2)	143.6(6)	O(1)#4-N(1)-O(1)	120(2)
O(3)-Pb(1)-Pb(1)#1	37.3(3)	Pb(1)-F(1)-Pb(1)#1	92.9(4)
F(1)-Pb(1)-Pb(1)#1	43.55(19)		

Symmetry transformations used to generate equivalent atoms:

#1 -x,-y+1,z #2 x+1,y,z #3 x-1,y,z #4 -x-1,y,z

Table S4. Anisotropic displacement parameters ($Å^2×10^3$) for $Pb_2(NO_3)_2(H_2O)F_2$

The anisotropic displacement factor exponent takes the form: $-2\pi^2 [h^2 a^{*2} U11 + ... + 2hka^* b^* U12]$

	U11	U22	U33	U23	U13	U12
Pb(1)	25(1)	18(1)	22(1)	-1(1)	0	0
O(1)	50(6)	33(6)	39(6)	23(14)	-12(13)	4(5)
O(2)	27(9)	23(9)	26(7)	10(7)	0	0
O(3)	21(11)	25(12)	13(8)	0	0	0
N(1)	18(9)	26(11)	25(7)	2(8)	0	0
F(1)	24(7)	38(9)	23(6)	0	-4(5)	0

Table S5. Bond valence calculation for $Pb_2(NO_3)_2(H_2O)F_2$

Atoms	O(1)	O(2)	O(3)	F(1)	∑cations
Pb(1)	0.264	0.309	0.607	1.004	2.184
N(1)	1.537	1.562	/	/	4.636
H(1)	/	/	0.791 [×2]	0.026 [×2]	0.843
∑cations	1.801	1.871	2.189	1.056	/

Table S6. Contribution of different geometrical factors (g_{ijk}) to structure criterion

Crystal (n)	g_{311}/n	g_{322}/n	g_{333}/n
$Pb_2(NO_3)_2(H_2O)F_2$ (n=4)	0.91	0.15	0.73

Table S7. Direction and magnitude of dipole moment of PbO_9F_2 polyhedrons

Species	D_x	D_y	D_z	Magnitude
$Pb(1)O_9F_2$	0.00063	-1.08696	-9.33157	9.39466
$Pb(2)O_9F_2$	0.00043	1.08682	-9.33181	9.39488
$Pb(3)O_9F_2$	0.00043	-1.08691	-9.33178	9.39487
$Pb(4)O_9F_2$	0.00063	1.08695	-9.33157	9.39466
PbO_9F_2 (in unit cell)	0.00212	0	-37.3267	37.57907

Table S8. Atom-cutting analysis and calculated SHG coefficients (pmV^{-1}) and refractive index at 1064 nm

	d_{31}	d_{32}	d_{33}	n_x	n_y	n_z	Δn
$Pb_2(NO_3)_2(H_2O)F_2$	4.5537	-1.5923	-2.8917	1.9558	1.7231	1.8997	0.23
NO_3	3.8505	-0.4605	-3.0801	1.6741	1.3662	1.5990	0.31
PbO_9F_2	4.194	-1.0237	-2.7746	1.9476	1.7187	1.8734	0.23
Pb	2.9495	-0.6983	-1.589	1.7343	1.5728	1.6857	0.16
F	2.327	-0.3412	-1.820	1.5656	1.4248	1.4931	0.14
$Ba_2(NO_3)_2(H_2O)F_2$	2.5314	-1.337	-2.031	1.6609	1.5429	1.6395	0.12

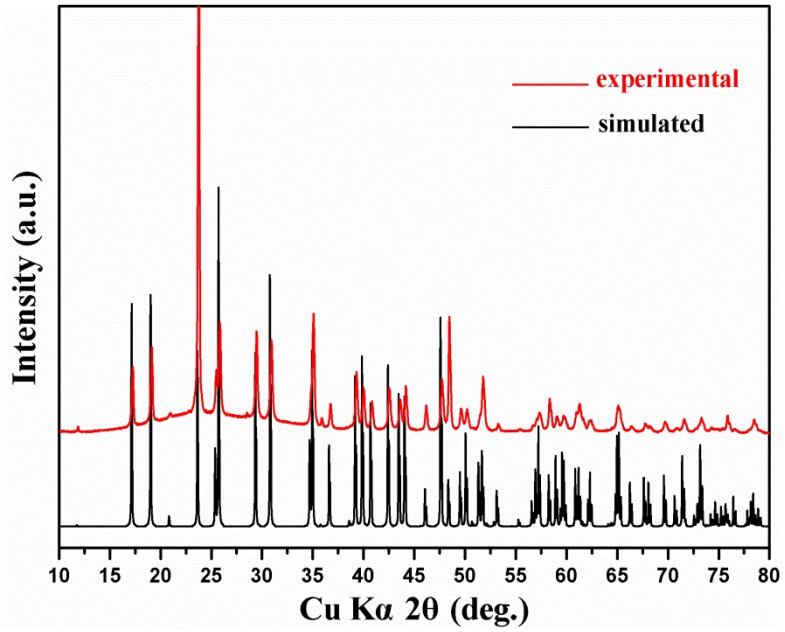

Figure S1. Simulated and experimental powder X-ray diffraction patterns of $Pb_2(NO_3)_2(H_2O)F_2$

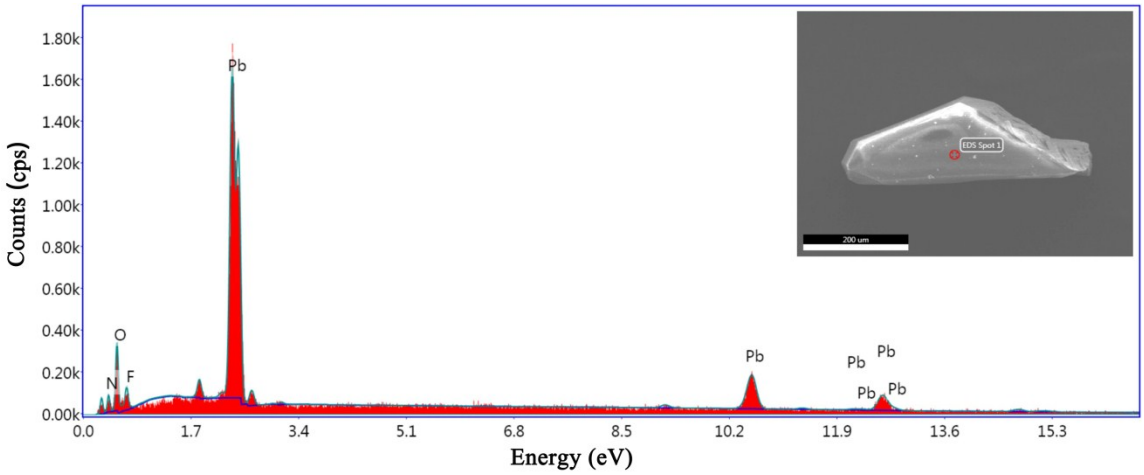

Figure S2. EDS analysis for $Pb_2(NO_3)_2(H_2O)F_2$. The inset is the SEM image of the tested crystal. Scale bar, 200 μm

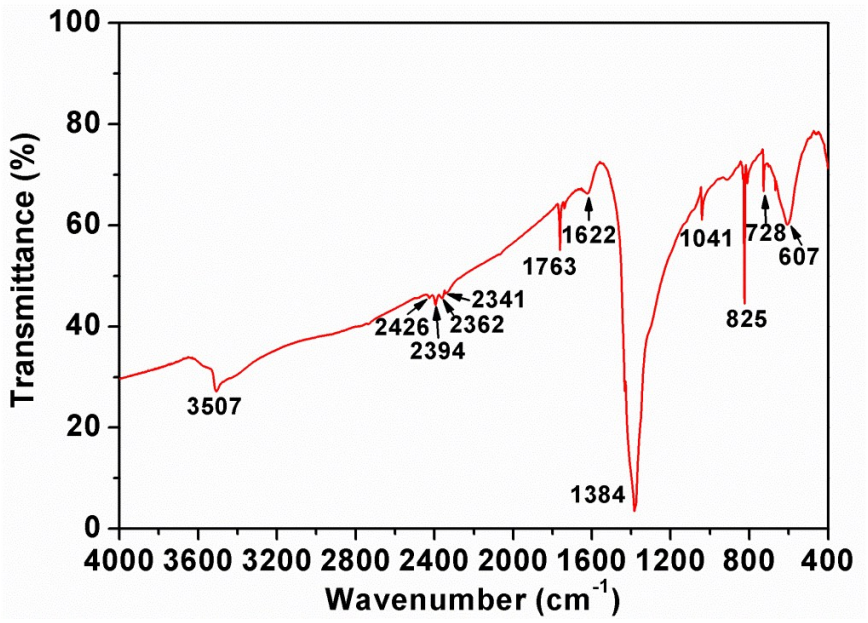

Figure S3. IR spectrum of $Pb_2(NO_3)_2(H_2O)F_2$

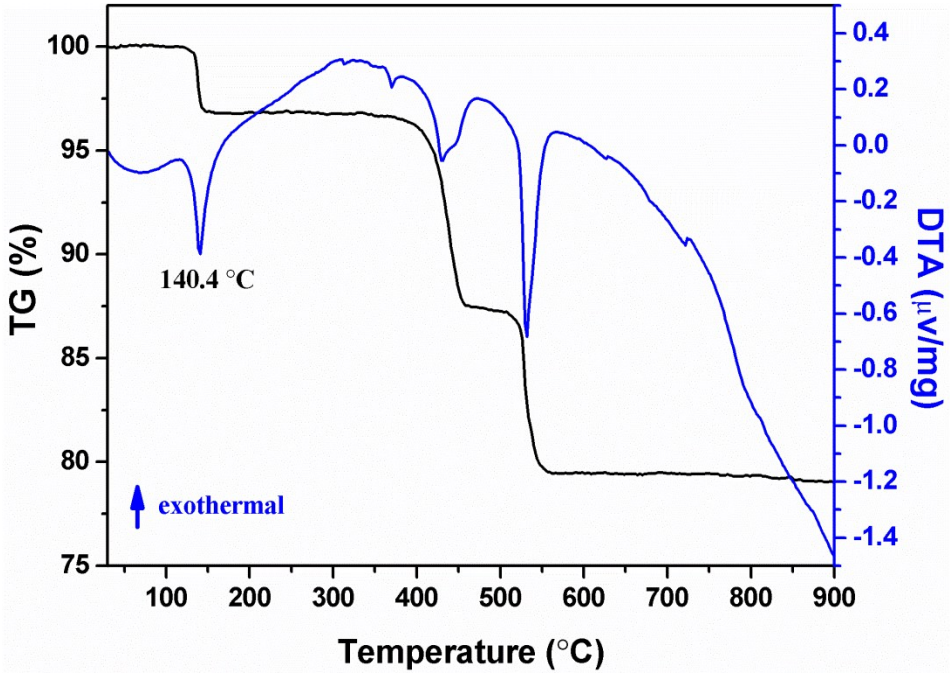

Figure S4. DTA and TG curves of $Pb_2(NO_3)_2(H_2O)F_2$

The TG and DTA curve reveals that $Pb_2(NO_3)_2(H_2O)F_2$ is stable up to 140 °C and the weight loss is in three steps. The first weight loss step is corresponding to the decomposition of one molecule of H_2O, showing a weight loss of 3.15% (calculated value 3.03%). The second and third steps from 350 °C to 600 °C are attributed to the decomposition of one molecule of N_2O_5, showing a weight loss of 17.55% (calculated value 18.17%).

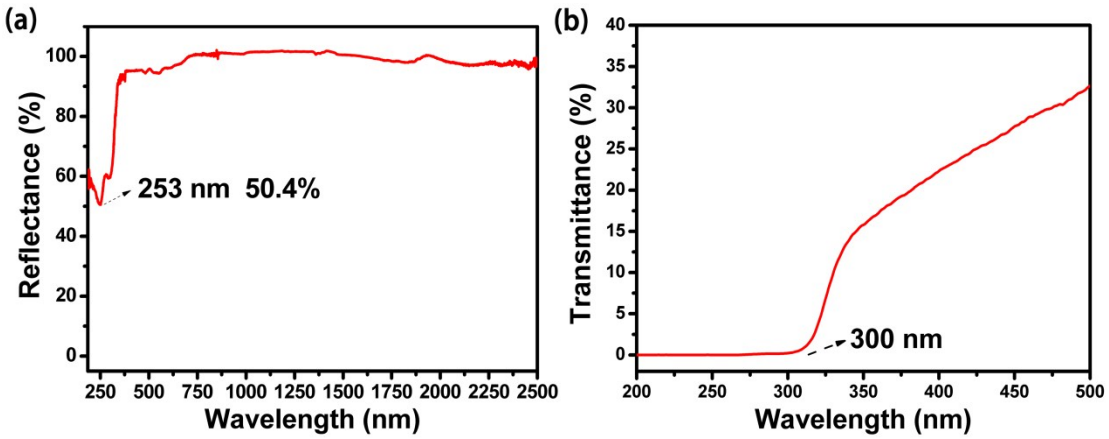

Figure S5. (a)Diffuse reflectance and (b) transmittance spectrum of $Pb_2(NO_3)_2(H_2O)F_2$

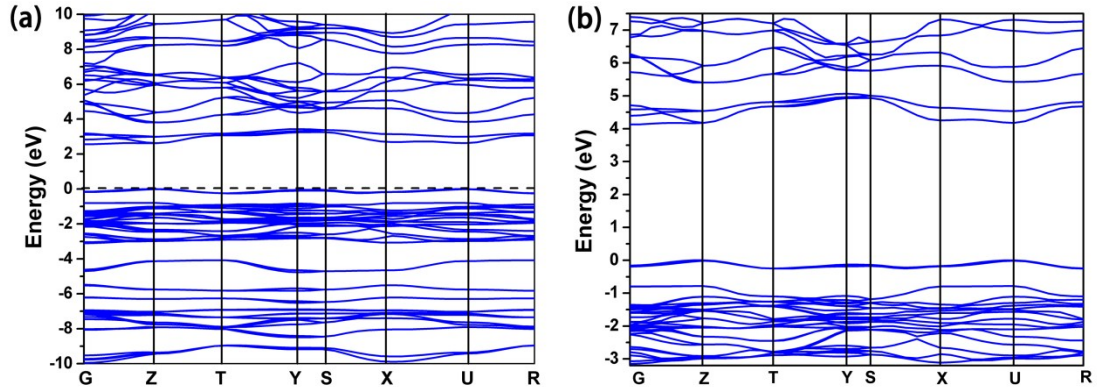

Figure S6. Calculated electronic band structures for $Pb_2(NO_3)_2(H_2O)F_2$ based on (a) DFT and (b) PBE0

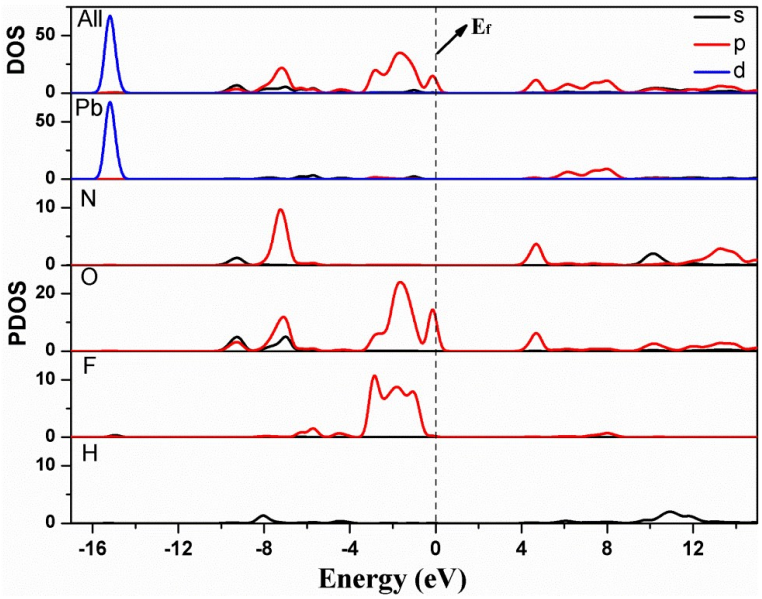

Figure S7. Total and partial DOS curves for $Pb_2(NO_3)_2(H_2O)F_2$. The E_f is displayed as a dashed vertical line and was used as a reference for all energy values (0 eV).

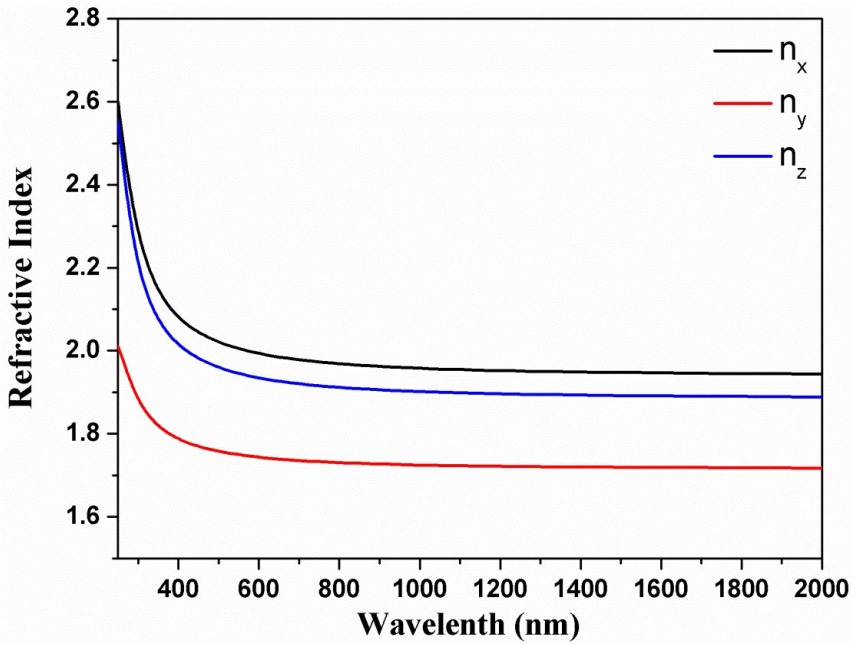

Figure S8. Dispersion curves of refractive index of $Pb_2(NO_3)_2(H_2O)F_2$

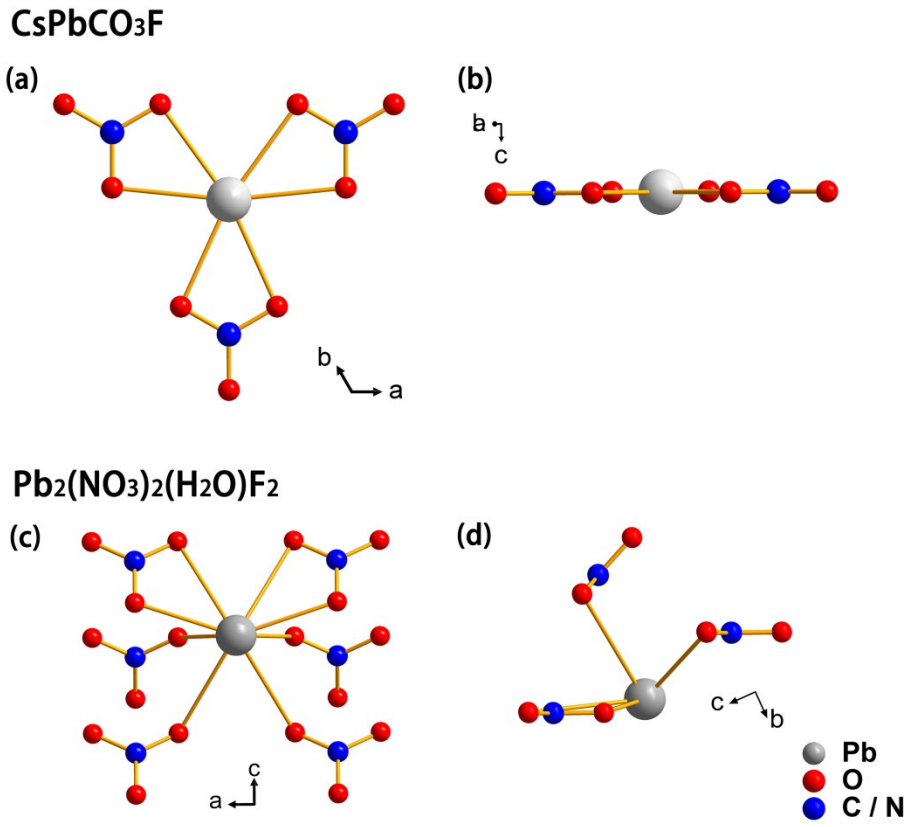

Figure S9. Structure comparison of $CsPbCO_3F$ and $Pb_2(NO_3)_2(H_2O)F_2$

Reference

1 G. M. Sheldrick, *Acta Crystallogr., Sect. A: Found. Crystallogr.* 2008, **64**, 112−122.
2 A. L. Spek, *J. Appl. Crystallogr.* 2003, **36**, 7−13.
3 S. K. Kurtz, T. T. Perry, *J. Appl. Phys.* 1968, **39**, 3798−3813.
4 S. J. Clark, M. D. Segall, C. J. Pickard, P. J. Hasnip, M. J. Probert, K. Refson, M. C. Z. Payne, *Z. Kristallogr. - Cryst. Mater.* 2005, **220**, 567-570.
5 M. C. Payne, M. P. Teter, D. C. Allan, T. A. Arias, J. D. Joan-nopoulos, *Rev. Mod. Phys.* 1992, **64**, 1045-1097.
6 J. P. Perdew, K. Burke, M. Ernzerhof, *Phys. Rev. Lett.* 1996, **77**, 3865-3868.
7 C. Adamo, V. Barone, *J. Chem. Phys.* 1999, **110**, 6158-6170.
8 A. M. Rappe, K. M. Rabe, E. Kaxiras, J. D. Joannopoulos, *Phys. Rev. B* 1990, **41**, 1227-1230.
9 L. Kleinman, D. M. Bylander, *Phys. Rev. Lett.* 1982, **48**, 1425-1428.
10 H. J. Monkhorst, J. D. Pack, *Phys. Rev. B* 1976, **13**, 5188-5192.
11 R. W. Godby, M. Schluter, L. Sham, *J. Phys. Rev. B* 1988, **37**, 10159-10175.
12 E. D. Palik, *Handbook of Optical Constants of Solids, Aca-demic Press*, 1985.
13 (a) J. Lin, M. H. Lee, Z. P. Liu, C. T. Chen, C. J. Pickard, *Phys. Rev. B* 1999, **60**, 13380-13389; (b) Z. S. Lin, X. X. Jiang, L. Kang, P. F. Gong, S. Y. Luo, M. H. Lee, *J. Phys. D: Appl. Phys.* 2014, **47**, 253001.
14 (a) I. D. Brown, D. Altermatt, *Acta Crystallogr., Sect. B: Struct. Sci.* 1985, **41**, 244−247; (b) N. E. Brese, M. Okeeffe, *Acta Crystallogr. B* 1991, **47**, 192-197.
15 C. T. Chen, Y. C. Wu, R. K. Li, *Int. Rev. Phys. Chem.* 1989, **8**, 65-91
16 N. Ye, Q. X. Chen, B. C. Wu, C. T. Chen, *J. Appl. Phys.* 1998, **84**, 555-558.